

pubs.acs.org/acssensors Article

# High Sensitivity Label-Free Quantitative Method for Detecting Tumor Biomarkers in Human Serum by Optical Microfiber Couplers

Youlian Wei, Wenchao Zhou,\* Yihui Wu,\* and Hongquan Zhu



Cite This: ACS Sens. 2021, 6, 4304-4314



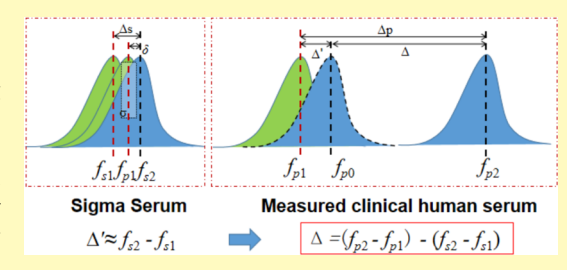
**ACCESS** 

Metrics & More

Article Recommendations

Supporting Information

ABSTRACT: Label-free optical fiber immunosensors have attracted wide-spread attention in recent decades due to their high sensitivity. However, nonspecific adsorption in serum has remained a critical bottleneck in existing label-free fiber optic biosensors, which hinders their widespread use in diagnostics. In addition, individual differences in clinical human serum (HS) negatively impact biosensing results. In this work, the modified serum preadsorption strategy was applied to reduce nonspecific adsorption by forming a saturated antifouling interface on an optical microfiber coupler (OMC). Furthermore, to reduce the effect of the differences between



individual HS samples, we proposed a new method where Sigma HS was used as a wavelength shift reference due to being close to clinical serum compared to other serums. Sigma HS was used first to reduce the differences in immune sensors before performing a clinical sample test in which quantitative detection was achieved based on the independent calibration of several sensors with wide dynamic ranges via dissociation processes. The individual differences in 25% HS were corrected by 30% Sigma HS. As a proof of concept, the label-free OMC immune sensor demonstrates good sensitivity and specificity for the detection of carcinoembryonic antigen (CEA) in 25% Sigma HS at different concentrations. The detection limit of CEA reached as low as 34.6 fg/mL (0.475 fM). Additionally, label-free quantitative detection of CEA using this OMC immune sensor was verified experimentally according to the calibration line, and the results agree well with clinical examination detection. To our knowledge, it is the first study to employ an OMC immune sensor in point-of-care label-free quantitative detection for clinical HS.

KEYWORDS: optical microfiber coupler, label-free, nonspecific adsorption, high sensitivity, quantitative detection, point-of-care

urrently, cancer is a global public health problem. Immunosensors with an ultralow detection limit for tumor biomarkers can promote early tumor screening, diagnosis, and postoperative recurrence monitoring. Carcinoembryonic antigen (CEA) has been identified as a biomarker for many cancers, including colorectal, breast, and lung cancers.<sup>2</sup> The clinical detection of the CEA content is beneficial for early cancer detection and disease progression diagnosis. Although conventional immunoassays such as ELISA<sup>3</sup> and chemiluminescence immunoassay<sup>4</sup> are widely used, they face the challenges of high costs and timeconsuming procedures, which limited their applicability in the field of point-of-care (POC) testing. To date, although many fluorescence or labeled sensing strategies for POC have been proposed, 5-9 the label-free method 10,11 is a good candidate in low-cost and simple operation.

Optical fiber sensors have been widely explored and applied in the field of biosensing 12-15 owing to their unique advantages of low cost, simple structure, and low electromagnetic interference. Compared with other optical fiber biosensors, the optical microfiber coupler (OMC) has the advantage of easy fabrication and high sensitivity. In particular, the OMC has attracted wide attention due to its ultrahigh sensitivity based on the interference turning point effect 16-18 in recent years. Although this kind of biosensor shows extraordinary

performance in biomolecule detection experimentally, to the best of our knowledge, the OMC biosensor has not been employed with clinical samples to date.

Nonspecific adsorption is inevitable <sup>19,20</sup> with the label-free detection of cancer markers in serum samples due to various proteins. There are many methods for overcoming the obstacle of nonspecific adsorption. For example, researchers have employed various nanomaterials, namely gold nanoparticles, <sup>21,22</sup> magnetic nanoparticles, <sup>23</sup> silica particles, <sup>24</sup> and quantum dots<sup>25</sup> that are decorated with secondary antibodies, to enhance specific binding signals and improve the signal-tonoise ratio so that the effects of nonspecific adsorption can be ignored. However, the sandwich immunoassay based on these nanomaterials requires additional time, cost, and operational procedures, and they also face the problems of poor repeatability of nanoparticles.

Received: May 18, 2021 Accepted: November 15, 2021 Published: November 20, 2021





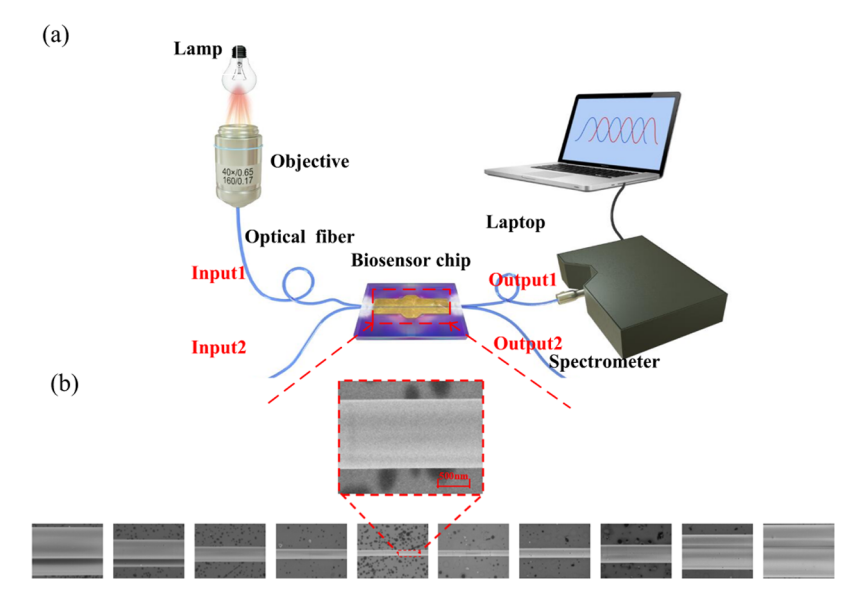


Figure 1. (a) Illustration of the experimental setup. (b) Optical micrograph of the optical fiber coupler.

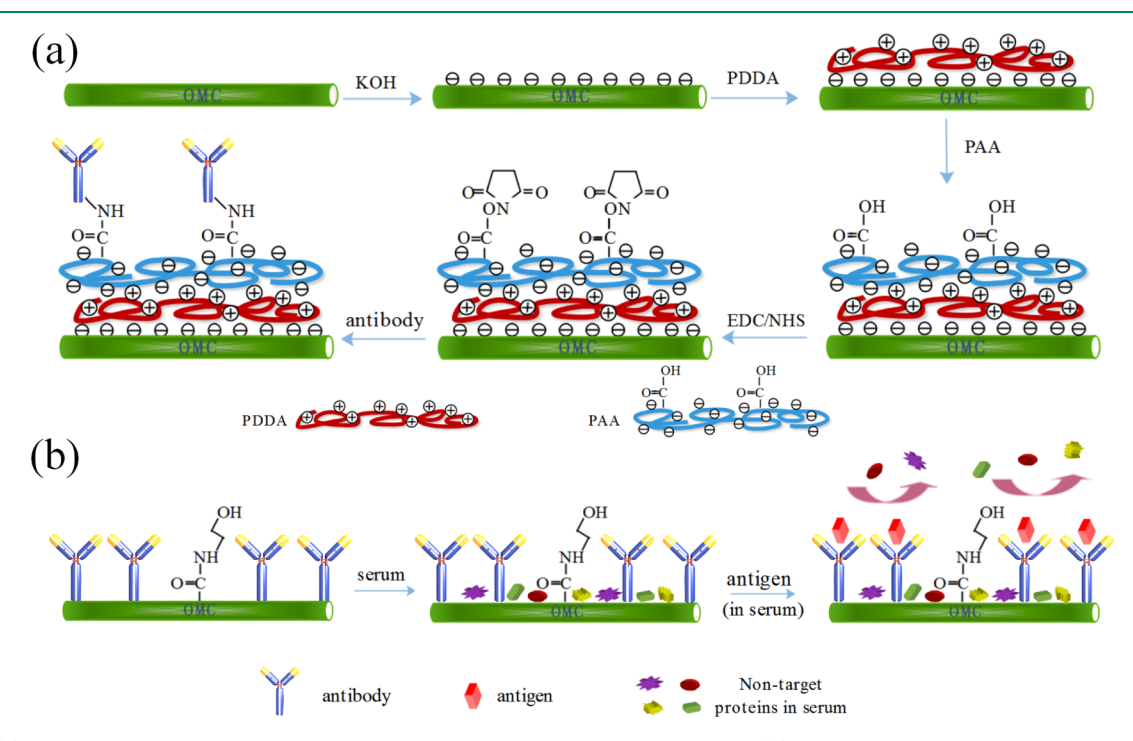


Figure 2. (a) Schematic illustration of antibody immobilization on the surface of the OMC. (b) OMC immunosensor blocking strategy diagram. The remaining activated carboxyl groups were deactivated by 1 M ethanolamine—HCl (pH = 8.5) to avoid more nonspecific protein combining with the rest of the group on the modified sensor and the preadsorption of serum as an antifouling interface on the functionalized OMC.

The use of resist nonspecific adsorption materials as the surface coating is the main strategy for the application of sensor label-free immunoassays in serum. <sup>26</sup> Polyethylene glycol and oligo-(PEG and OEG) motifs<sup>27–29</sup> are common choices, and zwitterionic polymers<sup>30–32</sup> are also good candidates that have been proven to possess notable antifouling properties. Another effective method to prevent nonspecific adsorption is to pretreat the sensor surface with serum. <sup>33–35</sup> Once the sensor surface is partially saturated with the adsorbed serum protein, then the rate of adsorption falls below the rate of diffusion, which has an inhibitory effect on adsorption. <sup>36</sup>

Although a few label-free detection strategies in clinical serum samples have been reported, <sup>37,38</sup> the interference caused

by individual differences in human serum (HS) for quantitative detection has not been resolved. This is one of the main obstacles for label-free biosensors to clinical application. In this work, the feasibility of the serum pretreatment strategy in label-free OMC immunosensors without antifouling materials was investigated, and a strategy based on the wavelength shift of Sigma HS was proposed to reduce the influence of individual differences in HS. The serum was diluted appropriately to reduce the effect of nonspecific adsorption. The blocking effects of different concentrations of serum samples and the conditions of serum stability were evaluated. The calibration curve was determined by high sensitivity and wide dynamic range detection of CEA in Sigma HS for several OMCs with

different sensitivities. Furthermore, the effect of different concentrations of Sigma HS on the correction of individual differences of HS was studied. To avoid the impact of sensor consistency, the OMC immune sensor needed to be calibrated independently first, and then, Sigma HS was used to correct individual differences in HS after dissociation. In this way, we demonstrated for the first time the label-free quantitative detection of CEA in HS based on OMCs. The results indicate that the OMC immunosensor has great potential in practical clinical diagnostics and POC testing.

#### MATERIALS AND METHODS

**Detection Mechanism of the Immunosensor.** By controlling the OMC to a certain diameter, low-order symmetry (even mode) and antisymmetric (odd mode) supermodes are excited at the same time. The interference phenomenon will occur when the odd and even modes propagate along the OMC so that an interferometric spectrum can be obtained at the output port.  $^{39}$  According to supermode theory, the output powers at through port  $P_3$  and cross port  $P_4$  are then given by

$$P_3 = P_1 \cos^2 \left(\frac{1}{2}\phi\right) \tag{1}$$

$$P_4 = P_1 \sin^2 \left(\frac{1}{2}\phi\right) \tag{2}$$

where  $\varphi$  represents the phase difference between the two supermodes accumulated along the coupling region for TE/TM polarization. The coupling coefficient of the OMC is dependent on the ambient refractive index (RI). The surface RI can be modified due to molecular binding on the OMC surface, resulting in a change in the output transmission spectrum. RI sensitivity can reach infinity when the difference between the effective exponents of the even mode and odd mode of the OMC is zero, which corresponds to the dispersion turning point.  $^{16,17}$ 

**Experimental Setup.** The experimental setup is shown in Figure 1a. The OMC was fixed in a fluid cell chip (Figure S1) for the delivery of sample solutions. A halogen lamp was used as the light source, and the light was launched into the fiber using a microscope objective with a numerical aperture of 0.65. A spectrometer with a resolution of 0.3 nm was used as the detector, and the data were acquired by a laptop. The wavelength range of the spectrometer is 600-980 nm. To eliminate the influence of temperature, the biosensing experiments were carried out in a clean room environment, and a temperature of  $23 \pm 0.2$  °C was maintained throughout the experiments (Figure S2). The microscope image of the OMC is shown in Figure 1b. The details of the preparation of optical fiber couplers are described in Supporting Information.

Biofunction and the OMC Immunosensor Assembly. The most common method for SiO<sub>2</sub> surface functionalization is silanization, 40 but this process will react with the chip material polymethyl methacrylate; therefore, the surface of the OMC was functionalized by the layer-by-layer (LBL) electrostatic selfassembly. 41-43 There are two layers of our bilayer system. As shown in Figure 2a, first, the OMC was cleaned with deionized water, and then, the OMC was immersed in 0.1 M potassium hydroxide (KOH) solution for 10 min to functionalize the OMC surface with OH groups. The OMC was then rinsed with deionized water. Next, charged surfaces were prepared by alternating incubation for 30 min with 2 mg/mL poly(diallyldimethylammonium chloride) (PDDA, positively charged) and 2 mg/mL poly(acrylic acid) (PAA, negatively charged). PDDA and PAA are prepared using deionized water. The negatively charged PAA is electrostatically adsorbed onto the positively charged PDDA. At the end of each step, the surface of the OMC was cleaned with deionized water. To facilitate covalent binding between the carboxyl group of PAA and amine groups of the antibody, the carboxyl group of PAA was activated by using a 1:1 mixture of 50 mM N-hydroxysuccinimide and 200 mM 1-(3dimethylaminopropyl)-3-ethalcarbodiimide hydrochloride for 30 min  $^{16}$  The immunosensor was then washed with PBS. Subsequently, the functionalized OMC was incubated with 100  $\mu$ L of antibody at room temperature for 2 h, followed by washing with PBS. When there are blank sites during the process of functional modification on the surface of the immune sensor or the antibody that do not completely cover the sensor surface, the complex proteins in the serum will absorb onto the blank surface of the sensor via hydrophobic, electrostatic, and exchange interactions between molecules and combine with the groups modified on the sensor surface.  $^{19,44-46}$  To further reduce nonspecific adsorption, the OMC was exposed to 1 M ethanolamine—HCl (pH = 8.5) for 30 min and blocked with Sigma HS for 30 min (Figure 2b), followed by washing with PBS. The volume of all reagents is 100  $\mu$ L to completely cover the OMC.

Antibody Concentration Selection. Nonspecific adsorption is closely linked to the amount of antibody immobilized on the biosensor surface. After the initial antibody concentration was immobilized, antibodies of different concentrations were added in sequence to investigate the deviation of the spectrum. First,  $100~\mu\text{L}$  of mouse monoclonal antibody against CEA (anti-CEA) with 100~ng/mL was immobilized on the surface of the OMC until reaction equilibrium was reached. After that,  $100~\mu\text{L}$  of anti-CEA with four concentrations (100~ng/mL,  $1~\mu\text{g/mL}$ ,  $10~\mu\text{g/mL}$ , and  $50~\mu\text{g/mL}$ ) continue to be added respectively, and the spectra red shift gradually as shown in Figure 3. After  $50~\mu\text{g/mL}$  anti-CEA has been added

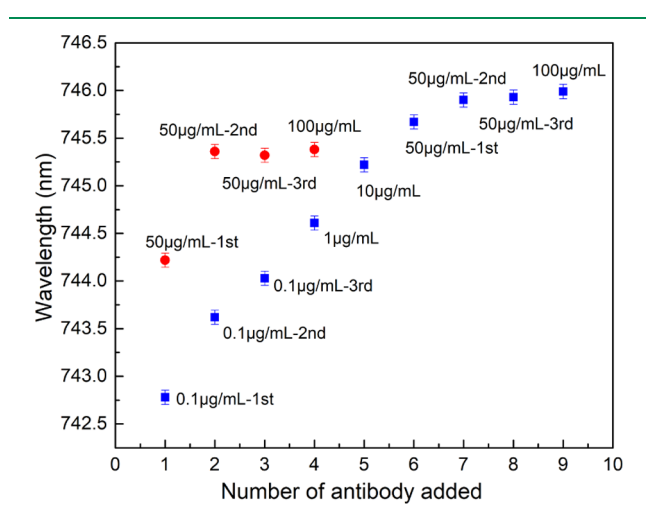


**Figure 3.** Dynamic processes and saturation of antibodies with different initial concentrations immobilized on the OMC.

repeatedly three times, 100  $\mu$ L of anti-CEA with 100  $\mu$ g/mL was added again. The wavelength will no longer move, which indicated that the reaction reaches saturation. Near the wavelength of 742 nm, the offset between 100 ng/mL and 100  $\mu$ g/mL is 3.1 nm, which shows that there are many remaining binding sites when immobilized with 100 ng/mL anti-CEA. Additionally, the reaction will reach saturation faster if the immobilized anti-CEA concentration has been raised to 50  $\mu$ g/mL. When the initial immobilized concentration was 50  $\mu$ g/mL, the wavelength shift was approximately 1.1 nm. The higher the initial concentration of immobilized antibody, the closer to saturation. To reduce the experiment cost, 10  $\mu$ g/mL anti-CEA was selected for immobilization. The remaining activated carboxyl groups were deactivated by 100  $\mu$ L of 1 M ethanolamine—HCl (pH = 8.5) for 30 min to avoid more nonspecific protein combining with the rest of the group on the modified sensor.

**Determination of Calibration Straight Line.** Each OMC immunosensor was individually calibrated. CEA was detected in 25% Sigma HS at different concentrations as an example. The concentration of the blocked serum should be higher than that of the tested serum. After blocking with 1 M ethanolamine—HCl (pH = 8.5), the OMC biosensor surface was blocked using 50% Sigma HS for 30 min. Then, the sensor surface was washed with PBS several

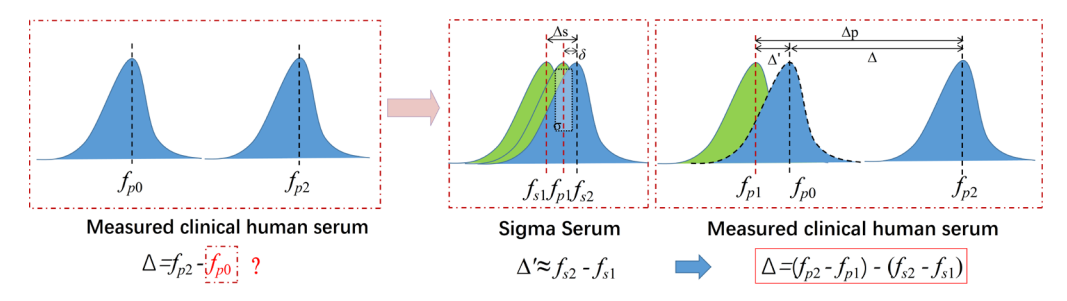


**Figure 4.** Schematic illustration of the specific signal extraction strategy for label-free quantitative detection.  $f_{p2}$  is the wavelength signal of the measured clinical HS at the end of the reaction,  $f_{p0}$  is the wavelength signal of the measured clinical HS without cancer markers at the end of the reaction,  $f_{p1}$  is the wavelength signal of the measured clinical HS at the beginning of the addition, and  $f_{s1}$  and  $f_{s2}$  represent the wavelength signals of Sigma HS at the beginning of the addition and at the end of the reaction, respectively.

times. The blank serum sample (25% Sigma HS) was subsequently added until three blank serum curves overlapped. The standard deviation  $\sigma$  of the overlapping blank serum curve is less than 0.2 nm at each working wavelength of the spectrometer. Finally, different concentrations of CEA proteins in 25% Sigma HS were gradually injected into the detection cell. In addition, the spectral deviation was recorded in real time. In our experiment, the overlapping curve of the blank serum samples can be considered as a test baseline due to the lack of an antigen. When the samples' signal is larger than the one of the blank serum, the wavelength shift can be regarded as the antigen—antibody binding events.

Correction for Individual Differences in HS. As shown on the left side of Figure 4, ideally, the antigen—antibody specific signal  $\Delta$  is

$$\Delta = f_{p2} - f_{p0} \tag{3}$$

where  $f_{p0}$  is the wavelength signal of the measured clinical HS without cancer markers at the end of the reaction and  $f_{p2}$  is the wavelength signal of the measured clinical HS at the end of the reaction. However, usually,  $f_{p0}$  is unknown. The wavelength signals at the beginning of the addition of  $f_{p1}$  for different measured clinical HS samples were inconsistent, the standard deviation  $\sigma$  is greater than 0.8 nm, and there is uncertainty in the deviation  $\delta$  between the overlapping Sigma HS values. This may be caused by the different contents of multiple proteins in different HS samples. Therefore, using a specific serum transmission spectrum as a baseline instead of  $f_{p0}$  would result in a large error. When the output spectra of the measured Sigma HS samples overlapped, there was an offset  $\Delta s$ . This offset may be due to the balancing of serum reactions on the optical fiber. Therefore, we consider using the wavelength shift as a reference to analyze the feasibility of practical application. Sigma HS was used as the standard serum. For the detection of clinical HS, the wavelength shift includes the equilibrium response of the serum and the antigen-antibody response. As shown on the right side of Figure 4, the wavelength shift of the antigen-antibody specific signal  $\Delta$  is

$$\Delta = f_{p2} - f_{p0} = f_{p2} - f_{p1} - \Delta' \tag{4}$$

where  $\Delta'$  can be regarded as the wavelength shift of clinical HS without cancer markers between the beginning and the end of the reaction

Due to individual differences in HS,  $\Delta'$  may be different. In this work, 25% of clinical HS samples were tested. The effects of different concentrations of Sigma HS on the correction of individual differences in 23 samples of 25% healthy HS were investigated. There may also be a small amount of cancer markers in the healthy HS. To avoid collecting antigen—antibody binding signals, the calibration of individual differences between the HS and standard serum was investigated by the OMC with a wide diameter. The corresponding Sigma HS with the smallest average value and standard deviation of relative wavelength deviation was selected to calibrate the individual differences of HS.

If the influence of individual HS differences is small, based on the optimized serum and taking the deviation of the standard serum as a reference,  $\Delta'$  can be expressed using the difference between Sigma HS

$$\Delta' \approx f_{\rm s2} - f_{\rm s1} \tag{5}$$

By taking a small variation from eq 4,  $\Delta$  can be expressed as

$$\Delta = (f_{p2} - f_{p1}) - (f_{s2} - f_{s1}) = \Delta p - \Delta s$$
 (6)

where  $f_{s1}$  and  $f_{s2}$  represent the wavelength signals of Sigma HS at the beginning of the addition and at the end of the reaction, respectively.

#### RESULTS AND DISCUSSION

Anti-nonspecific Adsorption Evaluation. For pretreatment with HS, the blocking effect with different concentrations of HS, such as 25 and 50%, 50% FBS, and 50% HS:10 mg/mL BSA (1:1), was studied. The results of the wavelength shift of each time testing sample (25% HS) relative to the first addition of testing samples are shown in Figure 5. When the OMC was

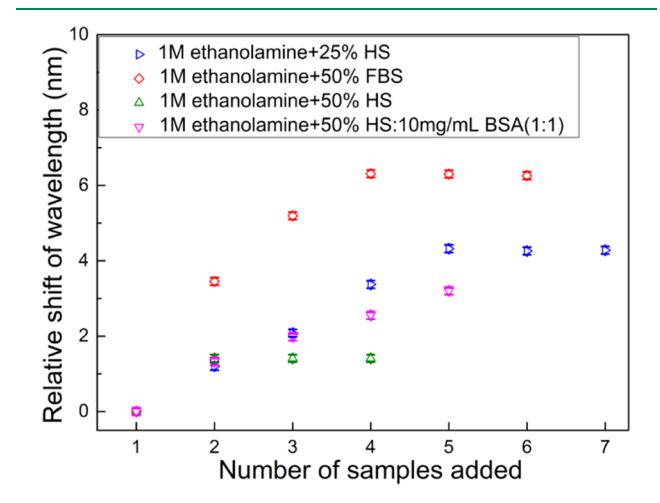


Figure 5. Overlapping situation of blank HS curves with different blocking strategies.

pretreated with 25% HS, the optical signal saturated after the fifth addition with a final wavelength shift of 4 nm. In contrast, the performance can be greatly improved if 50% HS has been adopted. This demonstrated that the optical wavelength remained steady after adding the second addition of the blank HS with a final wavelength shift of 1.5 nm. Each time the blank HS was added, the binding energy tends to decrease, and finally, the equilibrium state was reached. For 50% FBS, the signal saturates after the fourth addition with a final wavelength shift of 6 nm.

The results clearly indicate that the pretreatment with HS shows better anti-adsorption capability than FBS with the same concentration. This may be due to the historical dependence of

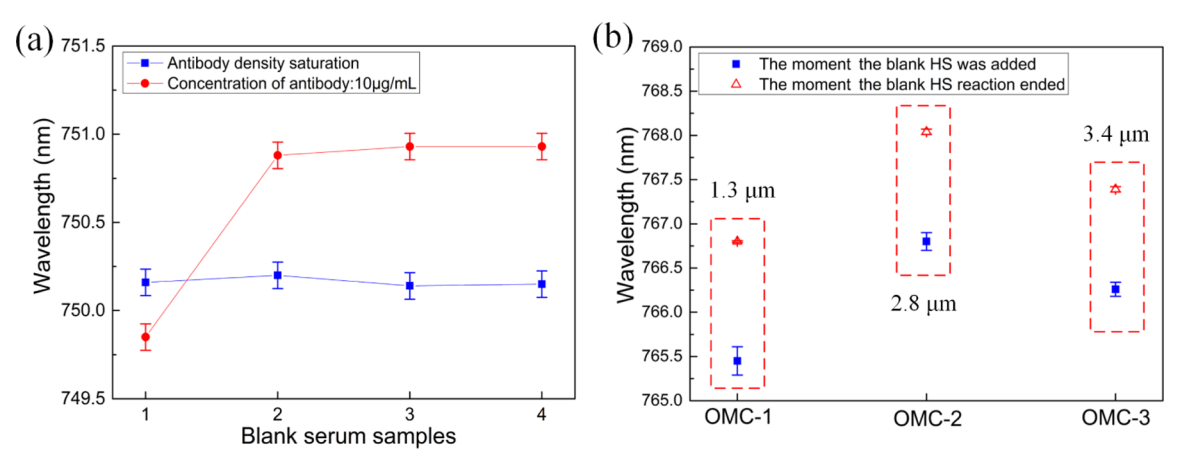


Figure 6. (a) Comparison of the deviation of blank serum samples under different antibody densities. (b) Wavelength shift of three applications of 25% Sigma HS following the second injection onto OMC surfaces with different diameters, corresponding to the sensitivity of 200 fg/mL, 200 pg/mL, and 2 ng/mL.

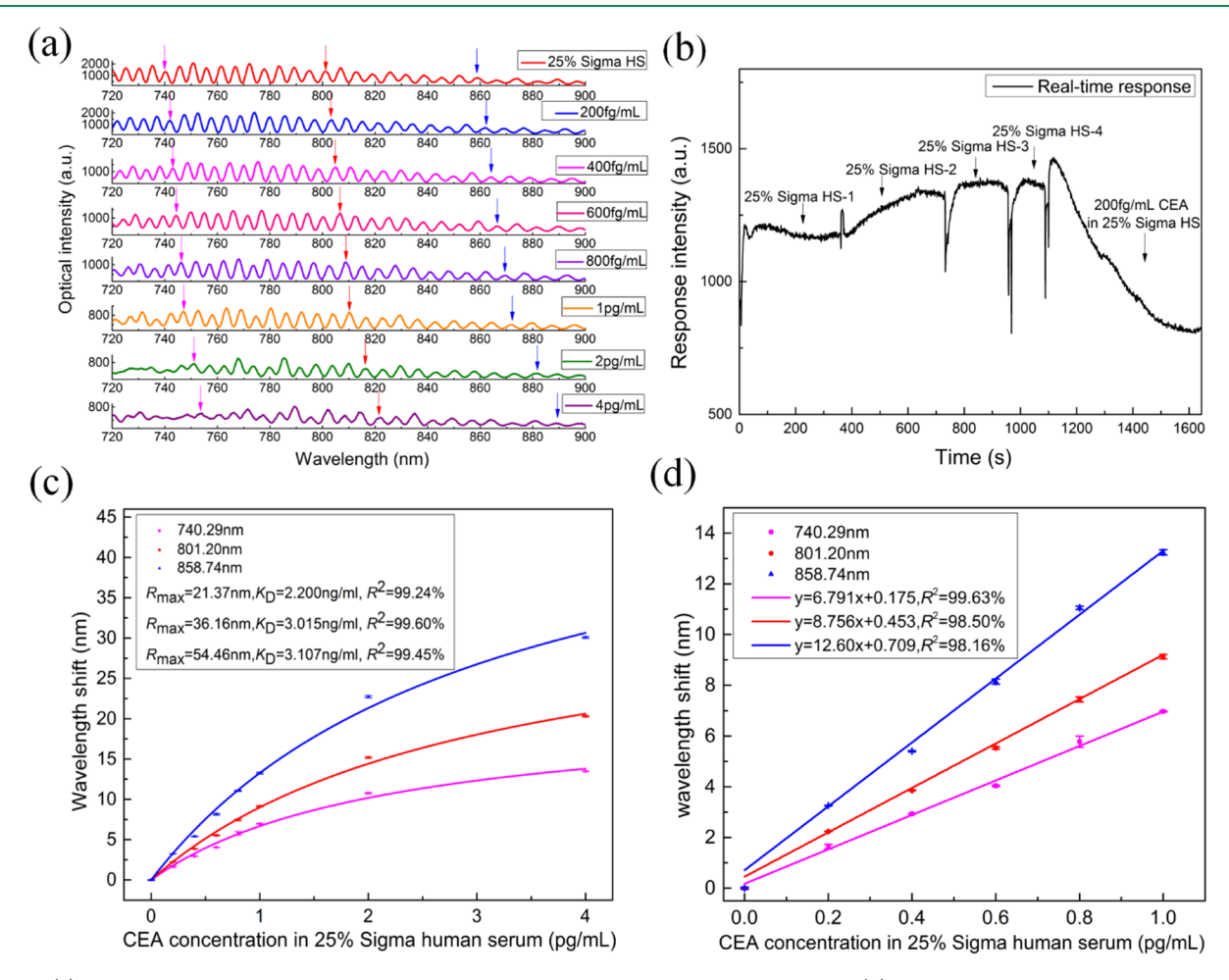


Figure 7. (a) Transmissive spectral response of 25% Sigma HS with different CEA concentrations. (b) Real-time dynamic response of the output transmission spectrum of 25% Sigma HS added successively 4 times and 200 fg/mL CEA in 25% Sigma HS in sequence. (c) Response of different concentrations of CEA in 25% Sigma HS (200 fg/m-4 pg/mL) binding to the anti-CEA immobilized on the surface of the OMC blocked with 50% HS. The solid line shows the least square fit of the Langmuir binding isotherm (n = 3). (d) Linear response of CEA in 25% Sigma HS binding to the anti-CEA immobilized on the surface of the OMC at a concentration in the range of 200 fg/mL-1 pg/mL (n = 3).

protein adsorption<sup>48</sup> and different adsorption rates of FBS and HS, which make the system tend to a new equilibrium.<sup>49</sup> When we blocked with 50% HS:10 mg/mL BSA (1:1), the effect was not better than blocked with 50% HS. The blocking effect is not as good as on the graphene surface,<sup>34</sup> which indicates that

it is related to the properties of adsorbent surfaces. <sup>50</sup> BSA has a higher binding affinity for hydrophobic surfaces than hydrophilic surfaces, which means that BSA is more easily exchanged on  ${\rm SiO}_2$  surfaces than graphene surfaces containing hydrophobic regions. <sup>51,52</sup>

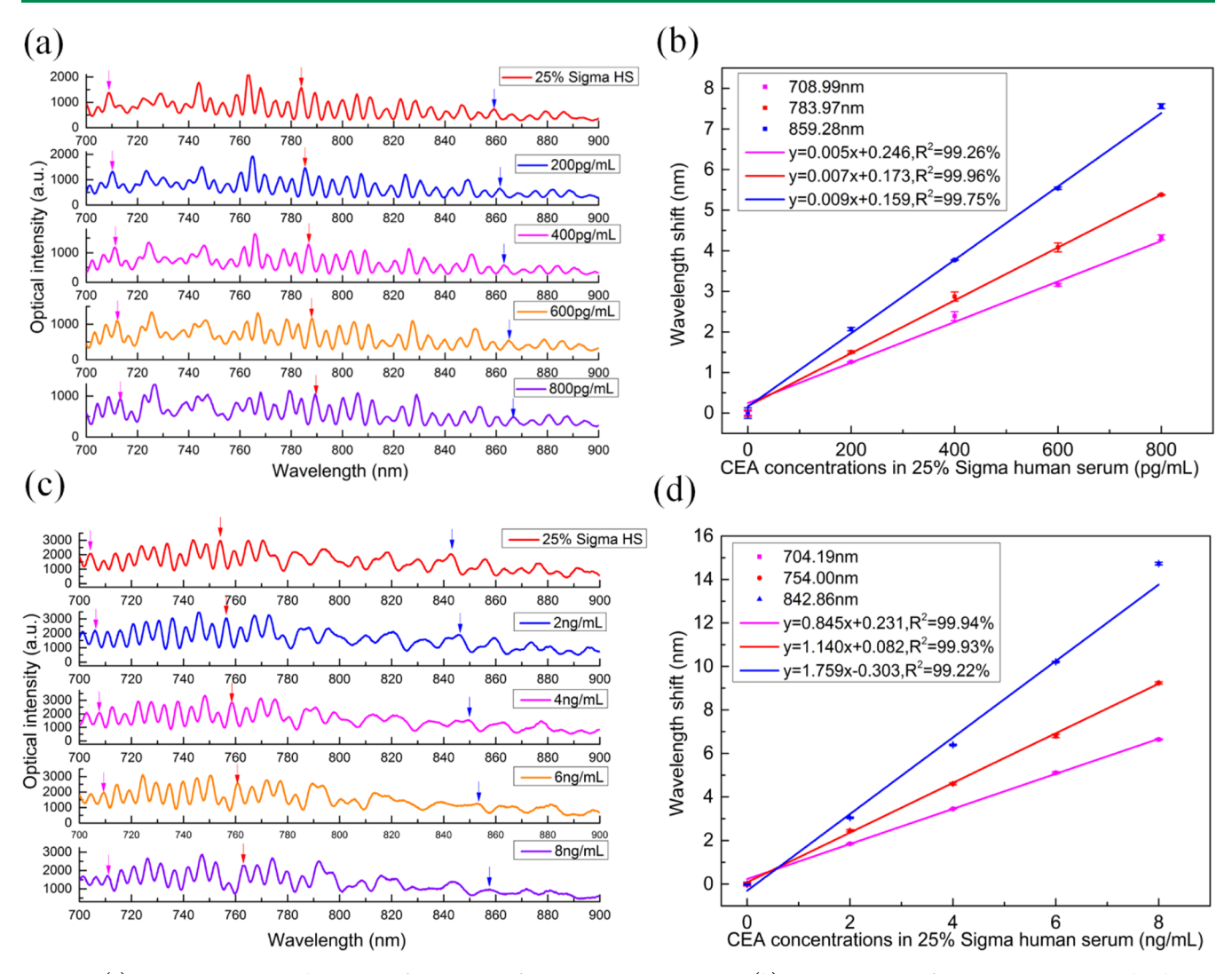


Figure 8. (a) Transmission spectral response of 200–800 pg/mL CEA in 25% Sigma HS. (b) Linear response of CEA in 25% Sigma HS binding to the anti-CEA immobilized on the surface of the OMC at a concentration in the range of 200–800 pg/mL (n = 3). (c) Transmission spectral response of 2–8 ng/mL CEA in 25% Sigma HS. (d) Linear response of CEA in 25% Sigma HS binding to the anti-CEA immobilized on the surface of the OMC at a concentration in the range of 2–8 ng/mL (n = 3).

The blank serum curves coincided after the addition of the second blank serum, which was equivalent to two serum occlusions fixed with 10  $\mu$ g/mL anti-CEA. When the antibody density is saturated (Figure 3), after blocking with 1 M ethanolamine—HCl (pH = 8.5) and 50% HS pretreatment, the blank HS curves overlapped after being added for the first time (Figure 6a). The higher the density of the antibody, the smaller the nonspecific adsorption. The serum saturates more quickly on the surface of the fiber.

According to our previous work, the sensitivity of the sensor increases as the fiber diameter decreases.  $^{16}$  Moreover, we show the anti-adsorption ability of 50% Sigma HS in the OMCs with different diameters. Three OMCs with diameters of 1.3, 2.8, and 3.4  $\mu$ m were prepared, which correspond to the sensitivity of 200 fg/mL, 200 pg/mL, and 2 ng/mL, respectively. The spectral responses of 25% Sigma HS showed differences due to the different RI sensitivities of OMCs. After adding 25% Sigma HS for the second time, the output spectra of OMCs with different diameters overlapped. The wavelength shift deviation of overlapping 25% Sigma HS samples was not significant. As shown in Figure 6b, near the wavelength of 766 nm, the standard deviation was 0.1 nm, and the average value was 1.24

nm. This was similar to the wavelength shift of the overlapping blank HS after the second addition in the case of antibody saturation. Although the serum curves overlapped after the first addition of the blank HS in the case of antibody saturation, the wavelength shift of the blank HS at the first time was greater than that of the overlapped blank HS after the second addition due to the RI difference between the air and serum.

pretreatment strategy, we further investigated the specific detection ability of our OMC sensor for the tumor biomarker CEA in serum samples. The overlapping curve of the blank serum was taken as the baseline, and the deviation of the spectra after reaction to each concentration of antigen relative to the baseline was recorded. The responses of 200 fg/mL-4 pg/mL CEA in 25% Sigma HS are shown in Figure 7. The transmission spectral responses at multiple moments were recorded, and the change in the interference peak was clearly identified compared to the initial moment. The real-time dynamic response of the output transmission spectrum of 25% Sigma HS added successively four times and 200 fg/mL CEA in 25% Sigma HS in sequence were obtained by monitoring the output intensity at a wavelength of 780 nm. As shown in

Figure 7b, the curve of 25% Sigma HS added for the second time deviated from the curve of 25% Sigma HS added for the first time. However, the light intensity was basically consistent with the light intensity of 25% Sigma HS added for the third and fourth times, indicating that the curves overlapped. Then, the overlapping curve was used as the baseline, and 25% Sigma HS was added with a concentration of 200 fg/mL CEA, which had a significant deviation from the baseline. Three interference peaks with different wavelengths were selected for tracking the peak shift. The least-square fit of the response curve was carried out by using the Langmuir binding isotherm model. 53

$$R = \frac{R_{\text{max}}C}{C + K_{\text{D}}} \tag{7}$$

where  $R_{\rm max}$ , C, and  $K_{\rm D}$  represent the sensor response at saturation, the concentration of the sample measured, and the equilibrium dissociation constant, respectively. The calculation formula of the limit of detection (LOD) can be expressed by the modified Langmuir binding isotherm model as follows

$$LOD = \frac{3\sigma \cdot K_{D,\lambda}}{R_{\max,\lambda} - 3\sigma}$$
 (8)

where  $R_{\text{max},\lambda}$  and  $K_{\text{D},\lambda}$  represent the response at saturation and the equilibrium dissociation constant at different wavelengths, respectively. The standard deviation  $\sigma$  of the overlapping blank serum curve is less than 0.2 nm at each working wavelength of the spectrometer, and the response deviation relative to the blank serum of the LOD should be not less than  $3\sigma$  (0.6 nm) at the detection wavelength. According to eq 8, the LOD values are 63.6 fg/mL (0.874 fM), 50.9 fg/mL (0.699 fM), and 34.6 fg/mL (0.475 fM) at the wavelengths of 740.29, 810.20, and 858.74 nm, respectively. The wavelength shift increases for the peak closer to the turning point, and the sensitivity is higher. 16 Correspondingly, a lower detection limit can be achieved. In addition, due to the incompatibility between high sensitivity and wide dynamic range, a single OMC cannot cover the entire measurement range, and we also achieved linear dynamic range detection of CEA in 25% HS with concentrations of 200-800 pg/mL and 2-8 ng/mL (Figure

**Specificity Evaluation in HS.** To further verify the feasibility of serum preadsorption, the specificity of the immunosensor was characterized. We immobilized anti-CEA on OMCs, and four nonspecific antigens, immunoglobulin G (IgG), C-reactive protein (CRP), α-fetoprotein (AFP), and prostate-specific antigen (PSA), were tested as controls. Two concentrations, 200 fg/mL and 10 ng/mL, were measured. After the blank HS curves overlapped, 100  $\mu$ L of IgG, CRP, AFP, PSA, and CEA in 25% Sigma HS was sequentially added. From the test results shown in Figure 9, relative to the blank serum curve at the same wavelength, the deviations of IgG, PSA, AFP, and CRP curves are less than 0.5 nm, which demonstrates the high specificity of the pretreatment strategy.

**Dissociation Regeneration Experiment.** Regeneration and reusability are important characteristics of biosensors. To confirm the repeatability of the biosensor, we use 0.1 M glycine—HCl buffer  $(pH=2.3)^{21}$  as regeneration buffer to separate the combined antigen—antibody complex after each immune response. The results of dissociation for 10 min each time are shown in Figure 10. In the first measurement of 2 ng/mL CEA in 25% Sigma HS, the wavelength offset near 850 nm

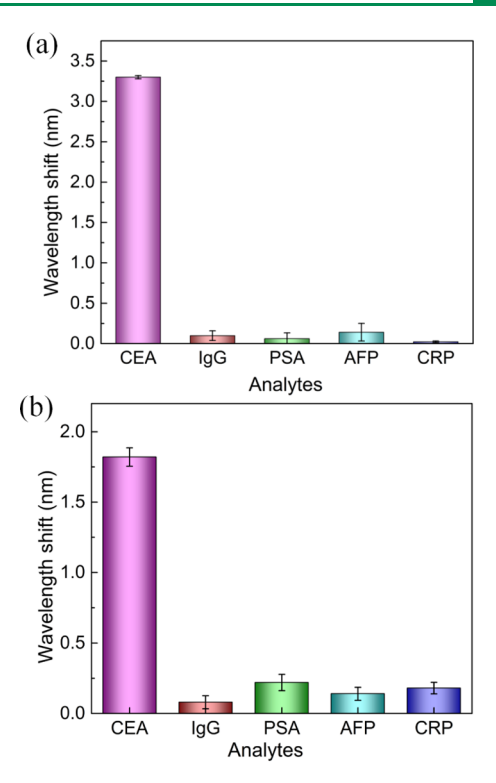


**Figure 9.** Measured response to CEA antigen and other nonspecific proteins at the same concentration (n = 3). (a) 200 fg/mL in 25% Sigma HS. (b) 10 ng/mL in 25% Sigma HS.

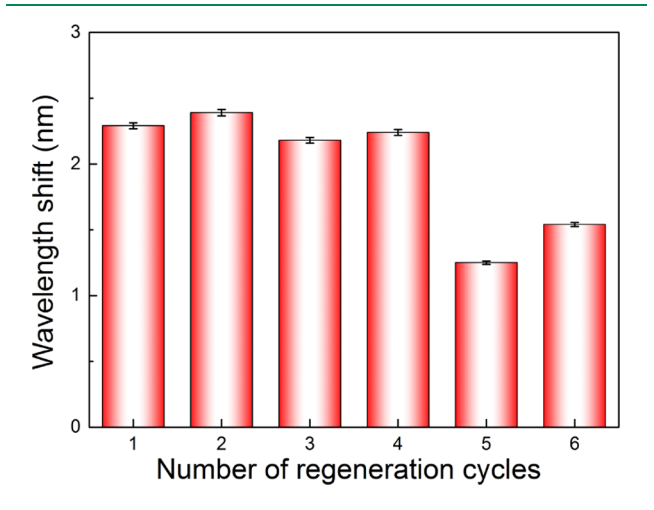


**Figure 10.** Repeatability of 2 ng/mL CEA in 25% Sigma HS, each dissociation time is 10 min.

was approximately 2.2 nm. After dissociating three times, the standard deviation of the first four detection results was less than 0.1 nm. However, after the fourth dissociation, the wavelength shift was approximately 1.3 nm, which significantly deviated from the first measurement result. The experimental results showed that when the 0.1 M glycine—HCl buffer solution (pH = 2.3) is dissociated for 10 min, the OMC can be used for four cycles (dissociating three times) repeatedly and there is no large error in label-free quantitative detection.

Label-Free Quantitative Detection of Clinical Serum Samples. Standard Serum Calibration for Individual Differences of HS. The wavelength shift of the second addition of Sigma HS was used to replace the wavelength shift of the clinical HS equilibrium reaction based on the result

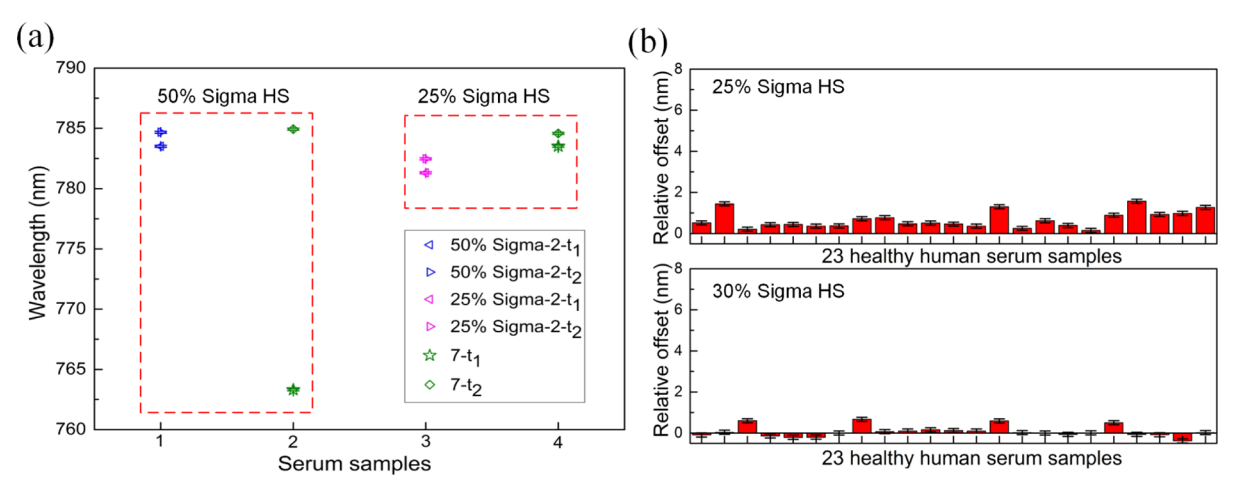


Figure 11. (a) Comparison of the wavelength shift of the second added Sigma HS ( $\Delta$ s) with that of no. 7 healthy HS ( $\Delta$ ') where  $t_1$  and  $t_2$  represent the start point and end point of the reaction, respectively. (b) Deviation of the wavelength shift between the second addition of Sigma HS ( $\Delta$ s) and 23 different healthy HS samples with a concentration of 25% ( $\Delta$ ').

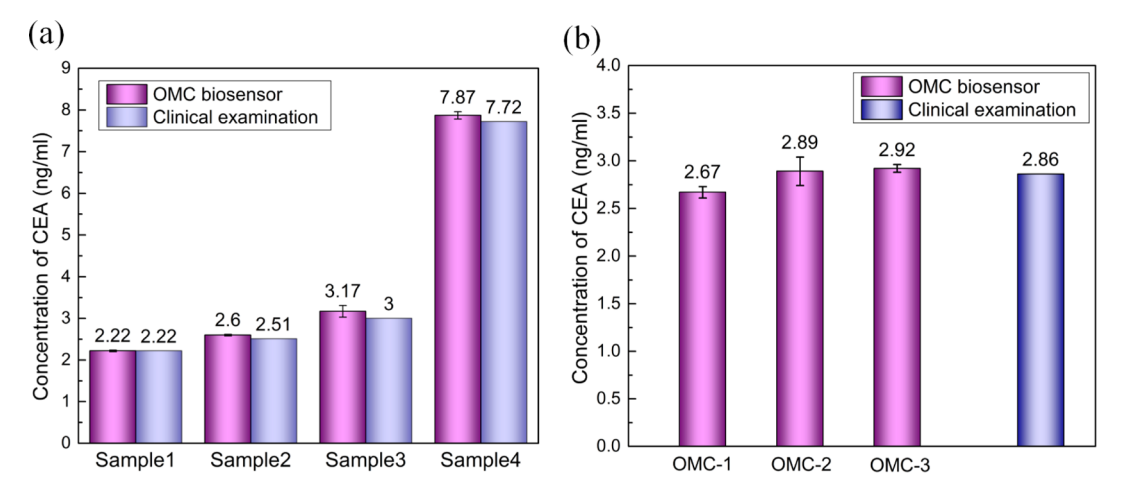


Figure 12. (a) Label-free quantitative detection results for CEA from four clinical HS samples using OMC immunosensors in comparison with clinical examination. (b) Label-free quantitative detection results for CEA from the same clinical HS sample by three OMC immunosensors in comparison with clinical examination.

of anti-nonspecific adsorption evaluation. According to eq 5, when the wavelength shift of overlapping Sigma HS was taken as a reference to reduce the influence of individual differences of HS, the wavelength shift deviation between Sigma HS and the healthy HS should be as small as possible. Blocking with 50% Sigma HS was performed, and then, the wavelength shifts of the second addition of 50, 25, and 30% Sigma HS and different 25% healthy HS samples were recorded and compared. As illustrated in Figure 11a, the wavelength shift of the no. 7 25% healthy HS sample was much larger than the wavelength shift of 50% Sigma HS. After the reaction, the spectrum of 25% healthy HS no. 7 was similar to that of 50% Sigma HS. In contrast, the spectrum was closer to the wavelength shift of 25% Sigma HS. This may be due to the difference between the 25% healthy HS and 50% Sigma HS being slightly larger, and the 25% healthy HS neutralized the 50% Sigma HS equilibrium response. With the OMC, the wavelength shifts of 23 healthy HS samples with a concentration of 25% were compared with the wavelength shifts of 25% Sigma HS added the second time. As shown in Figure 11b, the average value of the deviation was 0.64 nm, and the standard deviation was 0.42 nm near the wavelength of 710 nm. Compared with the wavelength shift following the

second addition of 30% Sigma HS, the average value was 0.08 nm, and the standard deviation was 0.27 nm near the wavelength of 710 nm. The experimental results indicate that 30% Sigma HS is more suitable as a reference to correct the individual differences of 25% HS, which satisfies eq 5. 30% Sigma HS is closer to 25% clinically healthy HS, and the dynamic equilibrium conditions on the fiber surface are similar. The deviation accounts for 2–7.5% of the entire OMC linear dynamic range.

Quantitative Detection of CEA in Clinical HS. To verify the proposed label-free quantitative method, the test results were compared with the clinical examination results. The clinical samples from the Second Hospital of Jilin University have been tested. The concentration of CEA in the samples was obtained using commercial chemiluminescence immunoassay (Beckman DXI800) first, and then, the samples were detected by the proposed quantitative method. First, various diameter OMC immune sensors with different sensitivities have been fabricated for different dynamic ranges. Then, calibration lines under different wavelengths can be obtained by detecting different concentrations of CEA in 25% Sigma HS. Next, 100  $\mu$ L of 0.1 M glycine—HCl buffer (pH = 2.3) was used to separate the combined antigen—antibody complex for 10 min.

The biosensor was washed with PBS, and 30% Sigma HS was added twice. Subsequently, 100  $\mu$ L of 25% clinical HS was added. The wavelength shifts of the second addition of 30% Sigma HS ( $\Delta$ s) and 25% clinical HS ( $\Delta$ p) were recorded. The biosensor was not washed during these steps. Taking the wavelength shift of the second increase as a reference, the antigen—antibody binding signal is represented by  $\Delta$ p— $\Delta$ s according to eq 6. Finally, the quantitative detection of CEA in different 25% clinical HS samples was realized according to the calibration line. The test results for each 25% clinical HS sample were multiplied by 4. As shown in Figure 12a, compared with clinical examination, the standard deviation for the detected results obtained using the OMC immunosensors was less than 5.7%, which demonstrates good consistency.

Furthermore, three different batches of OMCs with similar diameters were used to quantitatively detect CEA in the same clinical HS sample, and the clinical test result was 2.86 ng/mL. The experimental results shown in Figure 12b demonstrated that the standard deviation of the detection results for the OMC immunosensors was 0.14 ng/mL, the average value was 2.83 ng/mL, and the coefficient of variance (CV) was 4.9%, which indicated that the proposed label-free quantification method had good stability and reproducibility for detection of tumor biomarkers. The label-free quantitative detection strategy is also applicable to other optical fiber sensors.

# CONCLUSIONS

In this work, we demonstrated label-free quantitative detection of CEA in clinical HS based on OMC immunosensors for the first time, and the detection results were in good agreement with the clinical examination. Preadsorption on the surface of the OMC can be done using serum with a higher concentration than the measured one; therefore, the nonspecific adsorption can be significantly inhibited. The OMC immunosensors allowed the label-free detection of CEA in diluted serum with wide dynamic ranges. The results show that when the differences between the shifts of Sigma HS and healthy HS samples with the corresponding concentration are small enough, taking the wavelength shift of Sigma HS as a reference can greatly reduce the influence of individual differences in HS. The individual differences in 25% HS can be corrected by 30% Sigma HS, and the offset difference accounts for 2-7.5% of the entire OMC linear dynamic range. The quantitative detection of the wide dynamic range of CEA in HS can be achieved by several OMCs with different sensitivities according to this method. This work proved a great potential in POC clinical applications.

## ASSOCIATED CONTENT

# Supporting Information

The Supporting Information is available free of charge at https://pubs.acs.org/doi/10.1021/acssensors.1c01031.

Materials and reagents, preparation of optical fiber couplers, structure of the chip, temperature control, LBL assembly details, antibody fixation characterization, results of FBS preadsorption, and discussion of the LOD to the OMC (PDF)

# AUTHOR INFORMATION

#### **Corresponding Authors**

Yihui Wu — State Key Laboratory of Applied Optics, Changchun Institute of Optics, Fine Mechanics and Physics, Chinese Academy of Sciences, Changchun 130033, PR China; orcid.org/0000-0002-5289-3766; Email: yihuiwu@ciomp.ac.cn

Wenchao Zhou — State Key Laboratory of Applied Optics, Changchun Institute of Optics, Fine Mechanics and Physics, Chinese Academy of Sciences, Changchun 130033, PR China; Email: zhouvc@ciomp.ac.cn

#### **Authors**

Youlian Wei — State Key Laboratory of Applied Optics, Changchun Institute of Optics, Fine Mechanics and Physics, Chinese Academy of Sciences, Changchun 130033, PR China; University of Chinese Academy of Sciences, Beijing 100039, PR China

Hongquan Zhu – The Second Hospital of Jilin University, Changchun 130041, PR China

Complete contact information is available at: https://pubs.acs.org/10.1021/acssensors.1c01031

#### **Author Contributions**

Y.W. fabricated the OMC sensor, proposed the solution, performed the experiments and data analysis, and wrote the manuscript. W.Z. provided experimental guidance and method analysis and contributed to the manuscript. Y.W. proposed a label-free quantitative detection problem, provided a research program, and contributed to the characterization of the research results and manuscript. H.Z. collected clinical HS samples and data analysis.

#### Notes

The authors declare no competing financial interest.

# ■ ACKNOWLEDGMENTS

This work was supported by the National Natural Science Foundation of China (nos. 61974143, 61727813, and 61805241), Youth Innovation Promotion Association CAS (no. 2020223), and the Industrial Technology Research and Development Project of Jilin Province (no. 2019C035-2).

### REFERENCES

- (1) Sung, H.; Ferlay, J.; Siegel, R. L.; Laversanne, M.; Soerjomataram, I.; Jemal, A.; Bray, F. Global Cancer Statistics 2020: GLOBOCAN Estimates of Incidence and Mortality Worldwide for 36 Cancers in 185 Countries. *Ca-Cancer J. Clin.* 2021, 71, 209.
- (2) Washburn, A. L.; Gunn, L. C.; Bailey, R. C. Label-free quantitation of a cancer biomarker in complex media using silicon photonic microring resonators. *Anal. Chem.* **2009**, *81*, 9499–9506.
- (3) Acevedo, B.; Perera, Y.; Ruiz, M.; Rojas, G.; Benítez, J.; Ayala, M.; Gavilondo, J. Development and validation of a quantitative ELISA for the measurement of PSA concentration. *Clin. Chim. Acta* **2002**, 317, 55–63
- (4) Zhang, Y.; Xu, Q.; Peng, Q.; Cao, Z.; Wang, X.; Lu, J. Magnetic Beads-based Chemiluminescence Substrate-resolved Duplex Immunoassay for Sequential Detection of Two Ischemic Stroke Markers with Two Orders of Concentration Difference. *Anal. Sci.* **2011**, *27*, 739–743.
- (5) Ali, M.; Sajid, M.; Khalid, M. A. U.; Kim, S. W.; Lim, J. H.; Huh, D.; Choi, K. H. A fluorescent lateral flow biosensor for the quantitative detection of Vaspin using upconverting nanoparticles. *Spectrochim. Acta, Part A* **2020**, 226, 117610.
- (6) Wang, Q.; Li, R.; Shao, K.; Lin, Y.; Yang, W.; Guo, L.; Qiu, B.; Lin, Z.; Chen, G. A Portable Immunosensor with Differential Pressure Gauges Readout for Alpha Fetoprotein Detection. *Sci. Rep.* **2017**, *7*, 45343.

- (7) Ren, X.; Yan, J.; Wu, D.; Wei, Q.; Wan, Y. Nanobody-Based Apolipoprotein E Immunosensor for Point-of-Care Testing. *ACS Sens.* **2017**, *2*, 1267–1271.
- (8) Gao, Y.; Huo, W.; Zhang, L.; Lian, J.; Tao, W.; Song, C.; Tang, J.; Shi, S.; Gao, Y. Multiplex measurement of twelve tumor markers using a GMR multi-biomarker immunoassay biosensor. *Biosens. Bioelectron.* **2019**, *123*, 204–210.
- (9) Chen, Y.; Xianyu, Y.; Wu, J.; Dong, M.; Zheng, W.; Sun, J.; Jiang, X. Double-Enzymes-Mediated Bioluminescent Sensor for Quantitative and Ultrasensitive Point-of-Care Testing. *Anal. Chem.* **2017**, 89, 5422–5427.
- (10) Su, J.; Goldberg, A. F.; Stoltz, B. M. Label-free detection of single nanoparticles and biological molecules using microtoroid optical resonators. *Light Sci. Appl.* **2016**, *5*, No. e16001.
- (11) Yang, T.; Chen, S.; He, X.; Guo, H.; Sun, X. How to convincingly measure low concentration samples with optical label-free biosensors. *Sens. Actuators, B* **2020**, *306*, 127568.
- (12) Li, K.; Zhang, N.; Ying Zhang, N. M.; Zhou, W.; Zhang, T.; Chen, M.; Wei, L. Birefringence induced Vernier effect in optical fiber modal interferometers for enhanced sensing. *Sens. Actuators, B* **2018**, 275, 16–24.
- (13) Emiliyanov, G.; Høiby, P.; Pedersen, L.; Bang, O. Selective serial multi-antibody biosensing with TOPAS microstructured polymer optical fibers. *Sensors* **2013**, *13*, 3242–3251.
- (14) Liu, G.; Zhang, K.; Nadort, A.; Hutchinson, M. R.; Goldys, E. M. Sensitive Cytokine Assay Based on Optical Fiber Allowing Localized and Spatially Resolved Detection of Interleukin-6. ACS Sens. 2017, 2, 218–226.
- (15) Jeong, H.-H.; Erdene, N.; Park, J.-H.; Jeong, D.-H.; Lee, H.-Y.; Lee, S.-K. Real-time label-free immunoassay of interferon-gamma and prostate-specific antigen using a Fiber-Optic Localized Surface Plasmon Resonance sensor. *Biosens. Bioelectron.* **2013**, *39*, 346–351.
- (16) Zhou, W.; Li, K.; Wei, Y.; Hao, P.; Chi, M.; Liu, Y.; Wu, Y. Ultrasensitive label-free optical microfiber coupler biosensor for detection of cardiac troponin I based on interference turning point effect. *Biosens. Bioelectron.* **2018**, *106*, 99–104.
- (17) Li, K.; Zhang, T.; Liu, G.; Zhang, M.; Wei, L. Ultrasensitive optical microfiber coupler based sensors operating near the turning point of effective group index difference. *Appl. Phys. Lett.* **2016**, *109*, 101101
- (18) Zhang, L.; Tang, Y.; Tong, L. Micro-/Nanofiber Optics: Merging Photonics and Material Science on Nanoscale for Advanced Sensing Technology. *iScience* **2020**, *23*, 100180.
- (19) Choi, S.; Chae, J. Methods of reducing non-specific adsorption in microfluidic biosensors. *J. Micromech. Microeng.* **2010**, 20, 075015.
- (20) Lichtenberg, J. Y.; Ling, Y.; Kim, S. Non-Specific Adsorption Reduction Methods in Biosensing. *Sensors* **2019**, *19*, 2488.
- (21) Li, K.; Liu, G.; Wu, Y.; Hao, P.; Zhou, W.; Zhang, Z. Gold nanoparticle amplified optical microfiber evanescent wave absorption biosensor for cancer biomarker detection in serum. *Talanta* **2014**, 120, 419–424.
- (22) Kavosi, B.; Salimi, A.; Hallaj, R.; Moradi, F. Ultrasensitive electrochemical immunosensor for PSA biomarker detection in prostate cancer cells using gold nanoparticles/PAMAM dendrimer loaded with enzyme linked aptamer as integrated triple signal amplification strategy. *Biosens. Bioelectron.* **2015**, *74*, 915–923.
- (23) Krishnan, S.; Mani, V.; Wasalathanthri, D.; Kumar, C. V.; Rusling, J. F. Attomolar detection of a cancer biomarker protein in serum by surface plasmon resonance using superparamagnetic particle labels. *Angew. Chem., Int. Ed. Engl.* **2011**, *50*, 1175–1178.
- (24) Li, X.; Zhang, Y.; Xue, B.; Kong, X.; Liu, X.; Tu, L.; Chang, Y.; Zhang, H. A SERS nano-tag-based fiber-optic strategy for in situ immunoassay in unprocessed whole blood. *Biosens. Bioelectron.* **2017**, 92, 517–522.
- (25) Wang, H.; Wang, X.; Wang, J.; Fu, W.; Yao, C. A SPR biosensor based on signal amplification using antibody-QD conjugates for quantitative determination of multiple tumor markers. *Sci. Rep.* **2016**, *6*, 33140.

- (26) Vaisocherová, H.; Brynda, E.; Homola, J. Functionalizable low-fouling coatings for label-free biosensing in complex biological media: advances and applications. *Anal. Bioanal. Chem.* **2015**, 407, 3927–3052
- (27) Chen, R. J.; Bangsaruntip, S.; Drouvalakis, K. A.; Wong Shi Kam, N.; Shim, M.; Li, Y.; Kim, W.; Utz, P. J.; Dai, H. Noncovalent functionalization of carbon nanotubes for highly specific electronic biosensors. *Proc. Natl. Acad. Sci. U.S.A.* **2003**, *100*, 4984–4989.
- (28) Ma, S.; Li, X.; Lee, Y.-K.; Zhang, A. Direct label-free protein detection in high ionic strength solution and human plasma using dual-gate nanoribbon-based ion-sensitive field-effect transistor biosensor. *Biosens. Bioelectron.* **2018**, *117*, 276–282.
- (29) Sharma, R.; Deacon, S. E.; Nowak, D.; George, S. E.; Szymonik, M. P.; Tang, A. A. S.; Tomlinson, D. C.; Davies, A. G.; McPherson, M. J.; Wälti, C. Label-free electrochemical impedance biosensor to detect human interleukin-8 in serum with sub-pg/ml sensitivity. *Biosens. Bioelectron.* **2016**, *80*, 607–613.
- (30) Vaisocherová, H.; Yang, W.; Zhang, Z.; Cao, Z.; Cheng, G.; Piliarik, M.; Homola, J.; Jiang, S. Ultralow Fouling and Functionalizable Surface Chemistry Based on a Zwitterionic Polymer Enabling Sensitive and Specific Protein Detection in Undiluted Blood Plasma. *Anal. Chem.* **2008**, *80*, 7894–7901.
- (31) von Muhlen, M. G.; Brault, N. D.; Knudsen, S. M.; Jiang, S.; Manalis, S. R. Label-Free Biomarker Sensing in Undiluted Serum with Suspended Microchannel Resonators. *Anal. Chem.* **2010**, *82*, 1905–1910.
- (32) Wang, G.; Han, R.; Su, X.; Li, Y.; Xu, G.; Luo, X. Zwitterionic peptide anchored to conducting polymer PEDOT for the development of antifouling and ultrasensitive electrochemical DNA sensor. *Biosens. Bioelectron.* **2017**, *92*, 396–401.
- (33) Masson, J.-F.; Battaglia, T. M.; Khairallah, P.; Beaudoin, S.; Booksh, K. S. Quantitative Measurement of Cardiac Markers in Undiluted Serum. *Anal. Chem.* **2007**, *79*, 612–619.
- (34) Zhu, H.; Dale, P. S.; Caldwell, C. W.; Fan, X. Rapid and Label-Free Detection of Breast Cancer Biomarker CA15-3 in Clinical Human Serum Samples with Optofluidic Ring Resonator Sensors. *Anal. Chem.* **2009**, *81*, 9858–9865.
- (35) He, L.; Pagneux, Q.; Larroulet, I.; Serrano, A. Y.; Pesquera, A.; Zurutuza, A.; Mandler, D.; Boukherroub, R.; Szunerits, S. Label-free femtomolar cancer biomarker detection in human serum using graphene-coated surface plasmon resonance chips. *Biosens. Bioelectron.* **2017**, *89*, 606–611.
- (36) Andrade, J. D.; Hlady, V. Protein Adsorption and Materials Biocompatibility: A Tutorial Review and Suggested Hypotheses. *Adv. Polym. Sci.* **1986**, *79*, 1–63.
- (37) Mukundan, H.; Kubicek, J. Z.; Holt, A.; Shively, J. E.; Martinez, J. S.; Grace, K.; Grace, W. K.; Swanson, B. I. Planar optical waveguide-based biosensor for the quantitative detection of tumor markers. *Sens. Actuators, B* **2009**, *138*, 453–460.
- (38) Dey, P.; Fabri-Faja, N.; Calvo-Lozano, O.; Terborg, R. A.; Belushkin, A.; Yesilkoy, F.; Fàbrega, A.; Ruiz-Rodriguez, J. C.; Ferrer, R.; González-López, J. J.; Estévez, M. C.; Altug, H.; Pruneri, V.; Lechuga, L. M. Label-free Bacteria Quantification in Blood Plasma by a Bioprinted Microarray Based Interferometric Point-of-Care Device. ACS Sens. 2018, 4, 52–60.
- (39) Lacroix, S.; Gonthier, F.; Black, R. J.; Bures, J. Tapered-fiber interferometric wavelength response: the achromatic fringe. *Opt. Lett.* **1988**, *13*, 395–397.
- (40) Howarter, J. A.; Youngblood, J. P. Optimization of silica silanization by 3-aminopropyltriethoxysilane. *Langmuir* **2006**, 22, 11142–11147.
- (41) Korposh, S.; James, S.; Tatam, R.; Lee, S. Fibre-Optic Chemical Sensor Approaches Based on Nanoassembled Thin Films: A Challenge to Future Sensor Technology. *Curr. Dev. Opt. Fiber Technol.* **2013**, 237.
- (42) Yuk, J. S.; Guignon, E. F.; Lynes, M. A. Highly sensitive grating coupler-based surface plasmon-coupled emission (spce) biosensor for immunoassay. *Analyst* **2013**, *138*, 2576–2582.

- (43) Lai, X.; Gao, G.; Watanabe, J.; Liu, H.; Shen, H. Hydrophilic Polyelectrolyte Multilayers Improve the ELISA System: Antibody Enrichment and Blocking Free. *Polymers* **2017**, *9*, 51.
- (44) Raz, S. R.; Marchesini, G. R.; Bremer, M. G. E. G.; Colpo, P.; Garcia, C. P.; Guidetti, G.; Norde, W.; Rossi, F. Nanopatterned submicron pores as a shield for nonspecific binding in surface plasmon resonance-based sensing. *Analyst* **2012**, *137*, 5251–5259.
- (45) Cai, Y.; Schwartz, D. K. Influence of Protein Surface Coverage on Anomalously Strong Adsorption Sites. ACS Appl. Mater. Interfaces 2015, 8, 511–520.
- (46) Felgueiras, H. P.; Murthy, N. S.; Sommerfeld, S. D.; Brás, M. M.; Migonney, V.; Kohn, J. Competitive Adsorption of Plasma Proteins Using Quartz Crystal Microbalance. *ACS Appl. Mater. Interfaces* **2016**, *8*, 13207–13217.
- (47) Szöllősi, G. J.; Derényi, I.; Vörös, J. Reversible mesoscopic model of protein adsorption: From equilibrium to dynamics. *Phys. Stat. Mech. Appl.* **2004**, 343, 359–375.
- (48) Calonder, C.; Tie, Y.; Van Tassel, P. R. History Dependence of Protein Adsorption Kinetics. *Proc. Natl. Acad. Sci. U.S.A.* **2001**, 98, 10664–10669.
- (49) Kurrat, R.; Prenosil, J. E.; Ramsden, J. J. Kinetics of Human and Bovine Serum Albumin Adsorption at Silica—Titania Surfaces. *J. Colloid Interface Sci.* **1997**, *185*, 1–8.
- (50) Rabe, M.; Verdes, D.; Seeger, S. Understanding protein adsorption phenomena at solid surfaces. *Adv. Colloid Interface Sci.* **2011**, *162*, 87–106.
- (51) Green, R. J.; Davies, M. C.; Roberts, C. J.; Tendler, S. J. B. Competitive protein adsorption as observed by surface plasmon resonance. *Biomaterials* **1999**, *20*, 385–391.
- (52) Roach, P.; Farrar, D.; Perry, C. C. Interpretation of Protein Adsorption: Surface-Induced Conformational Changes. *J. Am. Chem. Soc.* **2005**, 127, 8168–8173.
- (53) Cooper, M. A. Label-Free Biosensors (Techniques and Applications); Springer, 2009.

